LANGMUIR

Interface Components: Nanoparticles, Colloids, Emulsions, Surfactants, Proteins, Polymers

Patterns Formation in Drying Sessile and Pendant Droplet: Interactions of Gravity Settling, Interface Shrinkage and Capillary Flow

Weibin Li, Wenjie Ji, Honghui Sun, Ding Lan, and Yuren Wang

Langmuir, **Just Accepted Manuscript** • DOI: 10.1021/acs.langmuir.8b02659 • Publication Date (Web): 07 Dec 2018

Patterns Formation in Drying Sessile and Pendant Droplet: Interactions of Gravity Settling, Interface Shrinkage, and Capillary Flow

Weibin Li, Wenjie Ji, Honghui Sun, Ding Lan*, and Yuren Wang†

National Microgravity Laboratory, Institute of Mechanics, Chinese Academy of Sciences, 100190 Beijing, China and School of Engineering Science, University of Chinese Academy of Sciences, 100049 Beijing, China

*landing@imech.ac.cn

†yurenwang@imech.ac.cn

Abstract

We reported the interactions of the gravitational sedimentation, the interface shrinkage and the outward capillary flow in drying droplets. This coupling effect is the inference we draw from deposition patterns of both sessile and pendant droplets, which contain particles of different sizes, evaporating on a patterned substrate. The deposition differnence between sessile and pendant droplet containing microparticles indicated that gravitational sedimentation has significant influence on the deposition morphology. A phase diagram shows that the particle deposition process can be divided into two stages: In the first stage, the competition between the interface shrinkage and the gravitational sedimentation determines whether the particles can be captured by the liquid-air interface. In the second stage, the capillary flow takes the particles inside the droplet towards the edge. The deposition morphology is the result of competition and cooperation interactions of the free setting, the interface shrinkage and the outward capillary flow.

Keywords: colloidal particles; pattern; capillary flow; coffee ring; droplet evaporation

Introduction

Drying of a colloidal droplet and the final deposition pattern are highly important in many biological and industrial applications such as DNA microarrays,[1-2] inkjet printing,[3-4] colloidal crystal formation,[5-7] disease diagnosis,[8-10] electronic devices,[11-12] and drug discovery.[13] However, it is difficult to control the droplet evaporation process artificially because many complicated physical phenomena are involved, including gravity-induced sedimentation, evaporative convection, surface-tension-driven flow, wetting and dewetting processes, the buoyancy effect, and diffusion of colloidal particles.[14]

A wide range of patterns can be left from the drying of a colloidal drop. The most observed deposition pattern, typically similar to a ring stain, is known as the 'coffee-ring' effect.[15] The coffee ring is usually induced by outward capillary flow, which would carry colloids towards the pinned contact line, eventually forming a ring-like stain.[16-17] The coffee-ring pattern can be reversed by the Marangoni effect, leading to a more uniform deposition pattern.[18] The Marangoni flow may be induced by temperature gradient or concentration gradient at the liquid–air interface of the droplet, which can substantially change the flow field and influence final deposition patterns.[19-21] Apart from convective flows, deposition patterns can be highly affected by many other factors, such as interface capture,[22-23] gravity sedimentation,[24-25] substrate wettability,[26-29] environmental pressure,[30] and particle size[31] and shape[32].

In fact, the above-mentioned physical effects are frequently involved simultaneously in the droplet evaporation process; therefore, the final deposition pattern should be determined by two or more such effects.[33-34] For instance, the coexistence of capillary and Marangoni flows during evaporation can render flow patterns of the drying droplet complex, further influencing deposition patterns.[35-37] Weon and Je[38] clarified a finger-pattern formation driven by competition between outward capillary flow and inward Marangoni flow. Nguyen et al.[23] found that the air–liquid interface capture effect can compete with the coffee-ring effect to manipulate colloidal residue deposits. Shen et al.[39] reported that the competition between time scales of liquid evaporation and particle movement influences ring formation. Bhardwaj et al.[40] showed that the shape of a colloidal deposit results from competition among three flow patterns: capillary flow, Marangoni recirculating flow, and Derjaguin–Landau–Verwey–Overbeek (DLVO) interactions.

Despite many studies emphasizing the interactions among different physical effects in drying droplets, a comprehensive understanding of such cooperative/competitive interactions on pattern formation is lacking. This paper investigates interactions of gravity settling, interface shrinkage, and capillary flow in the deposition patterns of evaporating droplets. Comparative studies were performed for sessile and pendant colloidal droplets. The influence of gravity on deposition morphology has been clarified. Furthermore, we propose a phase diagram and illustrate cooperative and competitive interactions among interface shrinkage, particle sedimentation, and capillary flow.

Experimental methods

Polystyrene (PS) colloidal particles, dispersed in pure water, were purchased from Duke Scientific Corporation and measured 300 nm, 500 nm, 700 nm, 1000 nm, 2200 nm, 3000 nm, and 6000 nm in diameter, respectively. The original mass concentration was 10 wt.% and nominal density was 1.05 g/cm^3. The monodisperse PS colloidal solution used in the experiment

was diluted to 0.1 wt.% with high-purity water. Prior to each experiment, the suspensions were stabilized using an ultrasonic cleaner (KQ2200DE, KUNSHAN ULTRASONIC INSTRUMENTS) for at least 10 min.

To ensure the sessile and pendant droplets each evaporated in constant contact radius (CCR) mode, we designed a patterned substrate with a circular hydrophilic region (7107 microscope slides, HAD) surrounded by a hydrophobic region (YC-AS coating, YuCrystal Encapsulation Company), as shown in Fig. 1. The dotted red circle represents the boundary of hydrophilic and hydrophobic regions. The radius of the hydrophilic region was chosen as 2 mm, 1.5 mm, and 0.9 mm. Each substrate was cleaned in an ultrasonic bath of alcohol and deionized water for 20 min successively and dried under a nitrogen stream. The contact angles for the hydrophilic and hydrophobic region were 5°and 115°, respectively; thus, a water-based droplet with the contact angle between [5°, 115°] could be restricted in the hydrophilic region. Considering the pinning effect for a droplet evaporating on a patterned substrate, the contact radius was kept constant, and the droplet evaporated in CCR mode. If the influence of gravity on droplet shape can be neglected, the shapes of the sessile and pendant droplets are similar. Detailed description about the patterned substrate and pinned droplet can be seen in our previous works.[41] Different volumes (20 μL, 10 μL, 3 μL) of diluted colloidal droplets were injected manually using micropipettes (DragonLAB, volume range: 0.5-10 μL, 5-50 μL) onto the patterned substrate.

Droplet shapes were captured with a Pentax DSLR Camera (K-30) equipped with a zoom lens (Pentax, DA 18-55mm f/3.5-5.6 AL) from a side view. The final deposition patterns were recorded using a microscope equipped with a digital camera (A1R-si, Nikon) from a bottom view. Images were analyzed in IMAGE-PRO PLUS 6.0 software. Experiments were repeated 3 times to establish reproducibility. All experiments were performed at an approximate environmental temperature of 25°C and 30% relative humidity. The uncertainty of measurement is below 2% for generated volume, 1.5% for static contact angle, and 5% for wetted radius.

Results and discussion

Experimental results

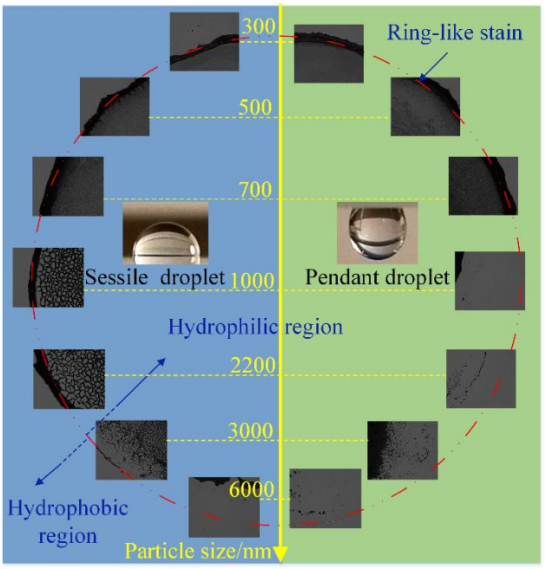

Figure 1. Deposition morphology near droplet edge after drying droplets with initial volume of 20 μL and concentration 0.1 wt.%; depositions at left blue and right green parts correspond to sessile and pendant droplets, respectively, which changed with particle size (300 nm, 500 nm, 700 nm, 1000 nm, 2200 nm, 3000 nm, 6000 nm). The red dotted circle line represents the interface between the hydrophobic and hydrophilic regions (with radius of 2 mm), where ring-like stains formed.

The aqueous colloidal droplets had the same initial concentration (0.1 wt.%) of PS micro- and nanoparticles. The evaporation of pendant and sessile colloidal droplets of different particle sizes (300 nm, 500 nm, 700 nm, 1000 nm, 2200 nm, 3000 nm, 6000 nm) on the same patterned substrate were studied simultaneously. The initial volume of the droplets was 20 μL, and the patterned substrate had a hydrophilic region with radius of 2 mm. After evaporating process was complete, the deposition morphology in the vicinity of the droplet periphery was recorded via microscopy, as depicted in Fig. 1. The red dotted circle line represents the position of the pinned contact line, where ring-like stains formed. The particle size increased along the vertical axis; depositions in the left blue and right green parts correspond to the sessile and pendant droplets, respectively. The deposition patterns for sessile and pendant droplets were entirely different. For sessile droplets, we observed a ring-like stain near the contact line for particle sizes between 300 and 3000 nm. The ring-like stain diminished for larger particles (6000 nm). The central deposition images were diverse for different particle sizes: nanoparticles (300 nm–700 nm) resulted in relatively uniform central depositions, whereas microparticles (1000–3000 nm) induced network-like patterns inside the ring. For pendant droplets, a ring-like stain was observed for nanoparticles only (300–700 nm); however, the ring vanished entirely for microparticles (1000–6000 nm). The central depositions of the pendant droplet also varied for different particle sizes: nanoparticles (300 nm–700 nm) resulted in more uniform depositions, and microparticles (1000–6000 nm) induced bumps. Comparing sessile and pendant droplets, the deposition patterns for nanoparticles were similar, but those for

microparticles were entirely different. These differences may result from a gravitational sedimentation effect or different droplet shapes.

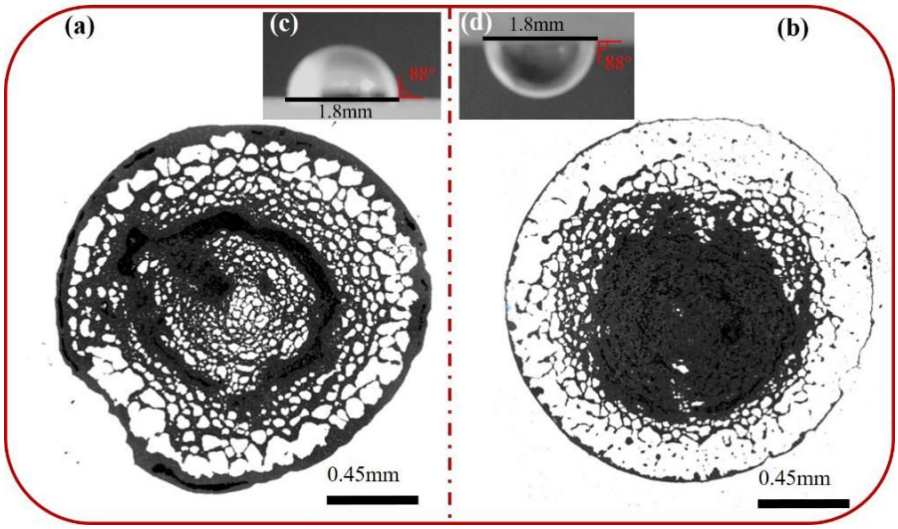

Figure 2. Deposition of drying small (initial volume: 3 μL) droplets containing 0.1wt.% PS microparticles (d = 2.2 μm) on patterned substrate (hydrophilic region with diameter of 0.9 mm). (a)–(b) are micrographs of deposition patterns for sessile and pendant droplets; (c)–(d) are side-view images of sessile and pendant droplets.

To further analyze the depositions of drying droplets, we used smaller droplets to eliminate the influence of droplet shape on the deposition pattern. The initial volumes of sessile amd pendant droplets (containing microparticles with sizes of 2.2 μm) were 3 μL with a contact radius of 0.9 mm. This droplet size was smaller than a characteristic length scale L, $L = \sqrt{\gamma / \rho g}$, labeled capillary length, where γ is the surface tension, ρ is the density of liquid, and g is the gravity acceleration (the capillary length of water is approximately 2.7 mm).[42] Thus, the gravitational influence on the droplet shape can be negligible. Furthermore, sessile and pendant droplets evaporated simultaneously in CCR mode under the same environmental conditions. Therefore, the shapes of the sessile and pendant droplets were identical, as presented in Fig. 2(c) and (d). The overall deposition patterns left by evaporation of the sessile and pendant droplets are shown in Fig. 2(a) and Fig. 2(b), respectively. The deposition patterns were distinct: for a sessile droplet, a typical ring-like stain was observed surrounding the central network pattern; for a pendant droplet, a weak ring-like stain was observed, with most particles aggregated at the center of the ring and forming a central bump. A more sparse network pattern was found between the ring-like stain and the central bump. Compared with the sessile droplet, the coffee-ring effect was greatly weakened for the pendant droplet, and the central stain was more concentrated. The formation of different deposition profiles can be ascribed to gravitational particle sedimentation, which is a unique variable among sessile and pendant droplets.

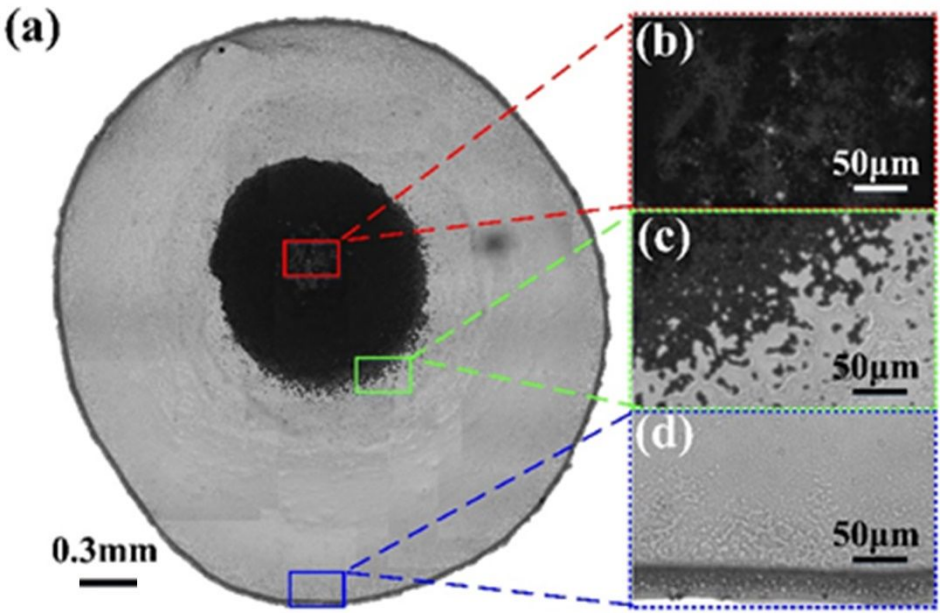

Figure 3. (a) Deposition patterns of binary colloidal solutions containing particles with sizes of 3000 nm (0.1 wt.%) and 300 nm (0.1 wt.%) after pendant droplet (with initial volume of 10 μL and contact radius 1.5 mm) evaporation; details of deposition morphology are in (b) the center region for microparticles, (c) the adjacent region between micro- and nanoparticles, and (d) the edge region for nanoparticles.

To further investigate the interactions of gravitional sedimentation and other effects, we conducted an experiment with an evaporating pendant droplet containing microparticles (d = 3000 nm) and nanoparticles (d = 300 nm). The initial volume of pendant droplet is 10 μL, and the radius of hydrophilic region is 1.5 mm. The final deposition patterns are depicted in Fig. 3(a), where the black and grey regions represent the deposition morphology of microparticles and nanoparticles, respectively. Figs. 3(b)–(d) are enlarged images of the red, green, and blue rectangular regions in Fig. 3(a) in sequence. Fig. 3(a) shows that nanoparticles formed central uniform depositions surrounded by a ring-like stain, whereas microparticles formed inner deposits consisting of monolayer or multilayer crystallites (Fig. 3[b]). A clear border appeared for depositions of nanoparticles and microparticles (Fig. 3[c]), and nearly no microparticles were deposited at the edge, as shown in Fig. 3(d).

Gravitational sedimentation effect

Gravity appeared to play a vital role in suppressing coffee-ring effects for the pendant droplet containing microparticles. The differences in deposition patterns of the sessile and pendant droplets may be due to either buoyancy-induced flow or Marangoni flow. However, the contribution of buoyancy to flow was considered negligible.[14] In addition, studies have shown that the Marangoni flow is weak in water droplets.[18] We observed recirculation flow on the surface of drying colloidal droplets at a large contact angle.[43] In this experiment, the Marangoni flow in sessile and pendant droplets was unlikely to be different; rather, we presume that Marangoni convection could accelerate particles close to the liquid–air interface to be captured by the interface, forming a quasi-steady-state monolayer island[22, 44] that prevents particles from escaping.

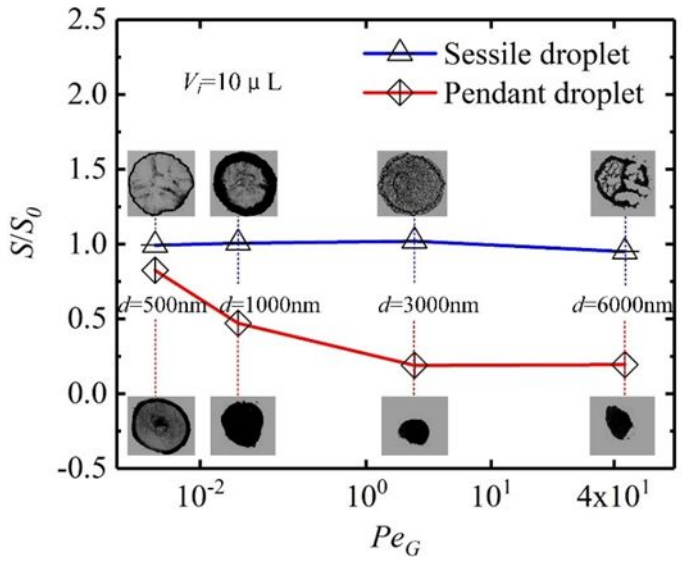

Figure 4. Ratio of deposition area and hydrophilic area (S/S_0) versus gravitational Pelect number (Pe_G, changed with particle sizes: 500 nm, 1000nm, 3000nm, 6000nm) for sessile (blue line) and pendant droplet (red line); the micrographs for each scatter point are visible (initial volume of the droplet is 10 μL, and radius of the hydrophilic region is 1.5 mm).

The only reason for differences in the deposition patterns between sessile and pendant droplets is the gravity effect. According to Devlin et al.[24] , sedimentation of large particles or aggregates is a dominating process in colloidal droplet evaporation, which could be described by the gravitational Peclet number:

$$Pe_G = \frac{\pi d^4 g \Delta\rho}{12 k_B T} \quad (1)$$

where d is the particle diameter, $\Delta\rho$ is the difference in density between particles and the surrounding fluid, g is gravitational acceleration, k_B is the Boltzman constant, and T is temperature. The gravitational Peclet number can be used to evaluate the relative contribution of gravitational sedimentation versus Brownian or thermal motion effects. The smaller the particle, the lower the Peclet number. Thus, small particles follow the streamlines closely, whereas larger particles can be easily dragged downward by gravity. Fig. 4 illustrates the ratio of the deposition area to the hydrophilic area (S/S_0) as a function of the gravitational Pelect number (P_{eG}) for a sessile droplet (blue line) and pendant droplet (red line). S/S_0 describes the extent to which particles were deposited on the substrate ($S/S_0 \leqslant 1$). As the Peclet number increased, S/S_0 remained nearly unchanged for the sessile droplet (blue line) but declined for the pendant droplet (red line).

When the Peclet number was small ($P_{eG} < 10^{-2}$), it formed a ring-like stain for the sessile and pendant droplets; gravitational sedimentation for nanoparticles can be negligible, leading capillary flow to dominate the deposition process. In another aspect, if the Peclet number were larger ($P_{eG} > 10^{-2}$), the deposition for sessile and pendant droplets would be totally different. For sessile droplets, a ring-like stain still existed while the deposition morphologies changed with an increase in the Peclet number, which remained relatively uniform for a larger Peclet

number. For pendant droplets, most particles aggregated and formed inner deposits, which became more concentrated as the Peclet number increased. The differences in deposition patterns for sessile and pendant droplets with a larger Peclet number can be attributed to gravitational sedimentation of microparticles. The microparticles settled down towards the substrate for sessile droplets, so most particles were deposited directly on the substrate and formed a relatively uniform deposition. By contrast, the microparticles settled towards the liquid–air interface and were captured in the central area for pendant droplets; thus, those captured particles were transferred from the liquid–air interface to the substrate and formed inner deposits. Although the influence of gravitational sedimentation on deposition patterns was analyzed, interactions among gravity and other effects in a drying droplet remained unclear and are further discussed in the next section.

Competitive and cooperative interactions

We developed a theoretical model to examine the relationship among gravitational sedimentation, interface shrinkage, and capillary flow in different evaporation stages. The three effects are important in a drying droplet. For an evaporating droplet, the terminal velocity of a particle falling downward in a fluid can be described by the Stokes law:[45]

$$u_p = \frac{d^2 \Delta\rho \mathrm{g}}{18\eta} \tag{2}$$

where u_p is the terminal velocity, d is the particle diameter, η is the viscosity, g is the gravitational constant, and $\Delta\rho$ is the difference in the density of the particle and the dispersed phase. As the particle size increases, the sedimentation rate increases and particles settle faster. The average interface shrinkage rate can be expressed as follows:[22]

$$u_i = \frac{h}{t_f} \tag{3}$$

where h is the initial height of the droplet; and t_f is the final evaporation time, which can be calculated if droplet evaporation is considered in a quasi-steady, diffusion-driven evaporation model.[46] The average interface shrinkage rate is determined by the droplet shape and evaporation rate. Capillary flow, caused by uneven evaporation flux on the droplet surface, will take particles from the center to the periphery. Close to the contact line, the height-averaged radial velocity u_c can be expressed by the following equation:[47]

$$u_c = \frac{D^*}{\theta} \frac{1}{\sqrt{R(\mathrm{R}-\mathrm{r})}} \tag{4}$$

where D^* is the diffusion coefficient, R is the contact radius of the drop, r is the distance from the drop center, and θ is the contact angle. There is an inverse correlation between the velocity of capillary flow and the contact angle. As mentioned earlier, the droplet evaporates in CCR mode, thereby strengthening capillary flow as the contact angle declines during the evaporation process.

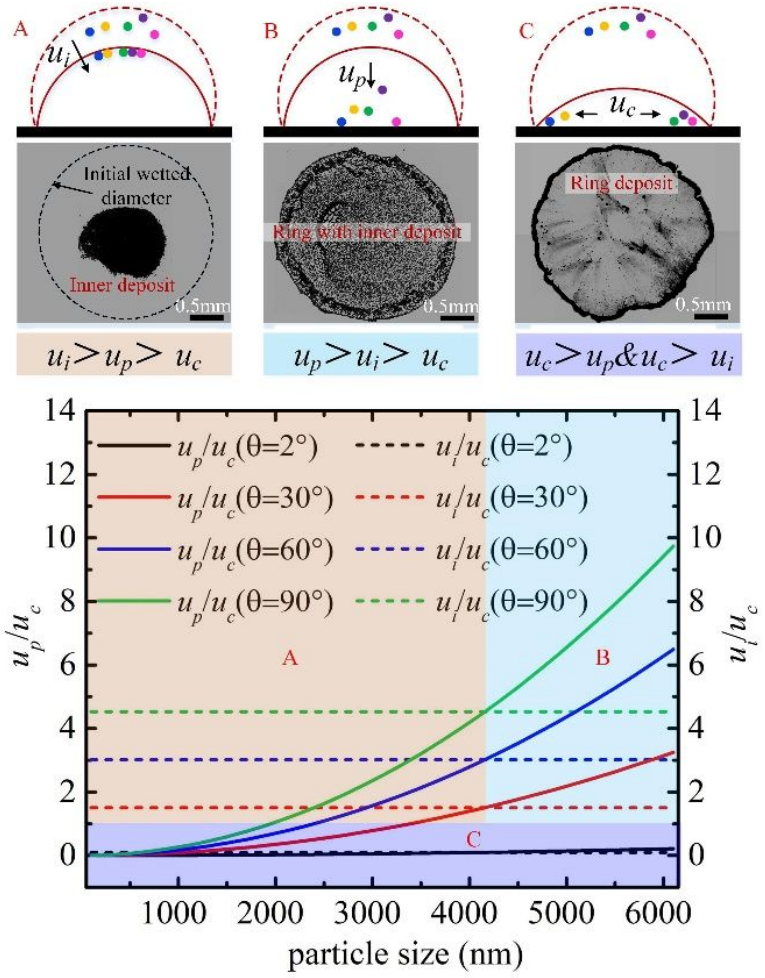

Figure 5. Variations in dimensionless numbers u_p/u_c (solid line) and u_i/u_c (dotted line) with particle size under different contact angles: 2° (black line); 30° (red line); 60° (blue line), and 90° (green line). The dominant regimes for u_i, u_p, u_c are represented in brown (regime A), blue (regime B), and purple (regime C) regions, respectively. In regime A, interface shrinkage rate is dominant ($u_i > u_p > u_c$), and particles are captured by the interface and form inner deposit. In regime B, the gravitational sedimentation is dominant ($u_p > u_i > u_c$), and particles settle downward and deposit on the substrate and form ring with inner deposit. In regime C, capillary flow plays a leading role ($u_c > u_p \& u_c > u_i$), and particles are pulled towards the contact line and form ring-like deposit.

The competitive effect between radial velocity and terminal velocity can be described as the dimensionless group number from Eqs. 2 and 4:

$$u_p / u_c = \frac{\Delta\rho \, g \sqrt{R(R-r)}}{18\eta D^*} d^2\theta \tag{5}$$

The ratio of interface shrinkage rate and radial velocity can be expressed through Eqs. 3 and 4:

$$u_i / u_c = \frac{\sqrt{R(R-r)}}{D^*} \frac{h\theta}{t_f} \tag{6}$$

We propose a phase diagram to predict deposit shapes from evaporated droplets containing colloidal particles. Considering this scenario in a specific experiment, we set $\eta = 0.89 \times 10^{-3}$Pa.s

in 25℃, R = 1.5 mm, ρ = 1050 kg/m^3, ρ_0 = 998 kg/m^3, D^* = 2.599 × 10^{-10} m^2/s,[47] g = 10 m/s^2, r = 0 mm, h = 3 mm, and t_f = 6000 s. Fig. 5 shows the ratios of u_p/u_c and u_i/u_c compared to particle size under different droplet contact angles. The diagram is divided into three regions (brown, blue, and purple), corresponding to three dominant regimes (A, B, and C) in the deposition process, respectively. In regime A, interface shrinkage rate was dominant (u_i>u_p>u_c) and particles close to the liquid–air interface were easily captured by the interface, these captured particles finally formed inner deposit, as shown in the micrograph in Fig. 5-A. In regime B, the terminal velocity of particles was dominant (u_p>u_i>u_c), so particles settled downward easily and deposited on the substrate, which eventually formed a ring with inner deposit, as presented in Fig. 5-B. In regime C, capillary flow played a leading role in particle deposition (u_c> u_p&u_c >u_i), such that particles were taken towards the contact line and formed ring-like deposit, as indicated in Fig. 5-C.

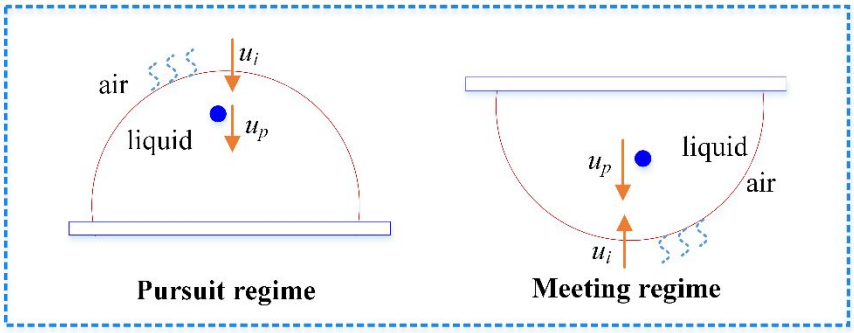

Figure 6. Schematic of pursuit regime and meeting regime for sessile and pendant droplets, respectively ($\Delta\rho > 0$).

The diagram in Fig. 5 reveals that the deposit shape results from the competition of three convective flow patterns: interface shrinkage, gravitational sedimentation, and capillary flow. During droplet evaporation, the particle deposition process can be divided into two stages. In the first stage, the contact angle was sufficiently large and capillary flow was weak, as shown in the brown and blue regions in Fig. 5. Two different regimes applied to sessile and pendant droplets at this stage: the pursuit regime and meeting regime, as pictured in Fig. 6. In the pursuit regime, the directions of interface shrinkage and particle sedimentation were each downward, suggesting that the descending interface was pursuing the particles. If $u_p > u_i$ (Fig. 5-B), the particles fell quickly and never came into contact with the liquid–air interface. Thus, parts of particles fell directly on the substrate while the other particles remained inside the droplet. If $u_p < u_i$ (Fig. 5-A), the interface could catch up with the particles and capture them. Then, one part of these particles accumulated at the interface, and the rest remained inside the droplet.In the meeting regime, the directions of interface shrinkage and particle sedimentation were opposite, indicating that the ascending interface tended to meet with the particles. If the $|u_p u_i|$ value was large, the interface met particles and captured them; nearly all particles accumulated and formed monolayer islands at the interface, as shown in Fig. 5-A. If the $|u_p u_i|$ value was small, the interface hardly came into contact with particles, and most remained inside the droplet.

Particles close to the liquid–air interface could be captured more quickly under the effect of recirculated Marangoni flow.[43] In the second stage, the contact angle was small and the outward capillary flow dominated particle motion (Fig. 5-C). Given sufficient particles inside the droplet, these particles were taken to the edge and formed a ring-like stain. Otherwise, particles trapped at the liquid–air interface were transferred directly to the substrate. When the contact angle was close to zero, the liquid film dewetting effect [43] or DLVO forces [40] could affect the final depositions.

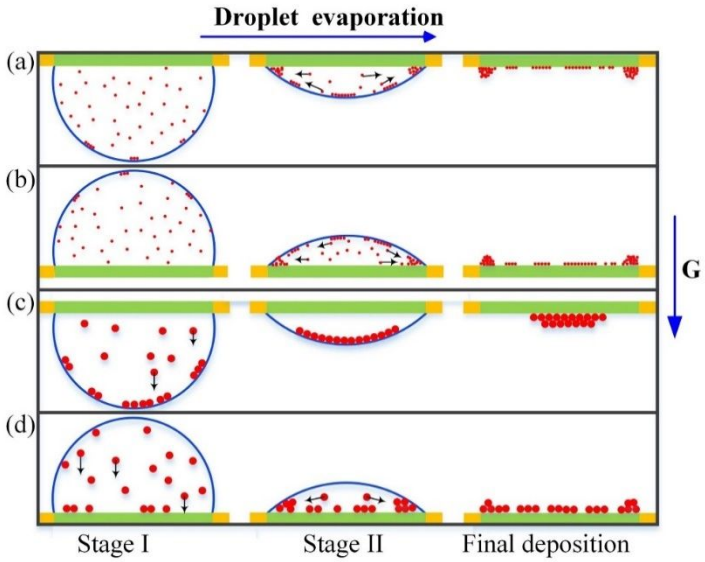

Figure 7. Formation mechanism of schematic of evaporation patterns of sessile and pendant droplets containing nanoparticles and microparticles. For (a) pendant or (b) sessile droplet containing nanoparticles, interface shrinkage and capillary flow dominate particle deposition and always form a ring with inner deposit. (c) For pendant droplet containing microparticles, interface shrinkage and gravitational sedimentation dominate particle deposition and eventually form an inner deposit. (d) For sessile droplet containing microparticles, gravitational sedimentation and capillary flow dominate particle deposition and finally form a ring with inner deposit.

The aforementioned theories explain the deposition of sessile and pendant droplets containing different sized particles. For example, for deposition patterns of a pendant droplet containing microparticles and nanoparticles (Fig. 3), microparticle settling and a rising liquid–air interface were concurrent and the $|u_p u_i|$ value was large, so nearly all settling microparticles were easily captured by the ascending interface, as shown in Fig. 7(c). Otherwise, fewer nanoparticles could be captured by the ascending interface because the $|u_p u_i|$ value was small, as depicted in Fig. 7(a). In the final evaporation stage (i.e., the period of outward capillary flow), nearly no microparticles were observed but many nanoparticles were left in the droplet. These trapped microparticles, which were prevented from moving towards the droplet edge, were transferred from the liquid–air interface to the substrate and aggregated into inner deposits, as shown in Fig. 3(a) and Fig. 7(c). However, nanoparticles inside the droplet could be taken by capillary flow to the edge to form a ring-like stain, as shown in Fig. 3(d) and Fig. 7(a). For

the sessile droplet, only some nanoparticles were captured by the descending surface ($u_p < u_i$), these trapped particles by the interface formed inner deposit; most nanoparticles inside the droplet were transported to the edge and formed a ring-like stain, as pictured in Fig. 7(b). However, most microparticles fell onto the solid–liquid interface under the action of gravity ($u_p > u_i$), these sedimentation particles finally formed deposition patterns inside the ring-like stain; other fewer microparticles were transported to the droplet edge under the effect of capillary flow and formed ring-like stain, as shown in Fig. 7(d). Compared with the model of particle deposition from drying sessile droplet established by Nguyen et al.[23], it was shown that both have a similar result in determining deposition patterns from competition between particles sedimentation and interface shrinkage. After calculating with the model by using our experimental data, the capture efficiency of the air/liquid interface of evaporating sessile droplet was equal to 95%, 87% and 2% as the particle diameter was 500 nm, 1000 nm, 3000 nm, respectively (the contact radius was chosen as 1.5 mm). Therefore, most of nanoparticles would be captured by the liquid-air interface, but few microparticles could be captured because of particle sedimentation due to gravity, which is consistent with our theoretical and experimental results of sessile droplet (Fig. 4).

Conclusions

In summary, we perform experiments on sessile and pendant colloidal droplets of various particle sizes. Results show similar ring-like stains and central depositions for sessile and pendant droplets containing nanoparticles, whereas these patterns were quite different for droplets containing microparticles. Pendant droplets formed a central deposition, and the ring vanished completely; for sessile droplets, the deposition was more uniform, and the ring still existed. The differences in deposition morphologies for microparticles were attributed to the gravitational sedimentation effect. We also propose a phase diagram and illustrate cooperative and competitive interactions of particle sedimentation, interface shrinkage, and capillary flow. The particle deposition process can thus be divided into two stages as with droplet evaporation. In the first stage, the competition between interface shrinkage and gravitational sedimentation determined whether particles could be captured by the liquid–air interface, which is the pursuit regime for sessile droplets and the meeting regime for pendant droplets. In the second stage, capillary flow dominated particle deposition and took particles inside the droplet towards the contact line.

Acknowledgements

We gratefully acknowledge financial support from National Natural Science Foundation of China (Grants No. U1738118 and No. 11472275), Strategic Priority Research Program on Space Science, the Chinese Academy of Sciences (A) (Grant Nos. XDA04020202, XDA04020406), and Strategic Priority Research Program of the Chinese Academy of Sciences (Grant No. XDB22040301).

References

1. Blossey, R.; Bosio, A., Contact line deposits on cDNA microarrays: a "twin-spot effect". *Langmuir* **2002,** *18* (7), 2952-2954.
2. Zhang, J.; Lettinga, P. M.; Dhont, J. K.; Stiakakis, E., Direct visualization of conformation and dense packing of DNA-based soft colloids. *Physical review letters* **2014,** *113* (26), 268303.
3. Zhang, L.; Liu, H.; Zhao, Y.; Sun, X.; Wen, Y.; Guo, Y.; Gao, X.; Di, C. a.; Yu, G.; Liu, Y., Inkjet printing high-resolution, large-area graphene patterns by coffee-ring lithography. *Advanced Materials* **2012,** *24* (3), 436-440.
4. Shimoni, A.; Azoubel, S.; Magdassi, S., Inkjet printing of flexible high-performance carbon nanotube transparent conductive films by "coffee ring effect". *Nanoscale* **2014,** *6* (19), 11084-11089.
5. Xia, Y.; Gates, B.; Yin, Y.; Lu, Y., Monodispersed colloidal spheres: old materials with new applications. *Advanced Materials* **2000,** *12* (10), 693-713.
6. Norris, D. J.; Arlinghaus, E. G.; Meng, L.; Heiny, R.; Scriven, L., Opaline Photonic Crystals: How Does Self-Assembly Work? *Advanced Materials* **2004,** *16* (16), 1393-1399.
7. Aguirre, C. I.; Reguera, E.; Stein, A., Tunable colors in opals and inverse opal photonic crystals. *Advanced Functional Materials* **2010,** *20* (16), 2565-2578.
8. Bou-Zeid, W.; Brutin, D., Effect of relative humidity on the spreading dynamics of sessile drops of blood. *Colloids and Surfaces A: Physicochemical and Engineering Aspects* **2014,** *456*, 273-285.
9. Zeid, W. B.; Brutin, D., Influence of relative humidity on spreading, pattern formation and adhesion of a drying drop of whole blood. *Colloids and Surfaces A: Physicochemical and Engineering Aspects* **2013,** *430*, 1-7.
10. Zeid, W. B.; Vicente, J.; Brutin, D., Influence of evaporation rate on cracks' formation of a drying drop of whole blood. *Colloids and Surfaces A: Physicochemical and Engineering Aspects* **2013,** *432*, 139-146.
11. Zhang, Z.; Zhang, X.; Xin, Z.; Deng, M.; Wen, Y.; Song, Y., Controlled inkjetting of a conductive pattern of silver nanoparticles based on the coffee-ring effect. *Advanced Materials* **2013,** *25* (46), 6714-6718.
12. Mampallil, D.; Eral, H. B., A Review on Suppression and Utilization of the Coffee-Ring Effect. *Advances in colloid and interface science* **2018**.
13. Zhang, D.; Xie, Y.; Mrozek, M. F.; Ortiz, C.; Davisson, V. J.; Ben-Amotz, D., Raman detection of proteomic analytes. *Analytical chemistry* **2003,** *75* (21), 5703-5709.
14. Lin, Z., *Evaporative self-assembly of ordered complex structures*. World Scientific: 2012.
15. Deegan, R. D.; Bakajin, O.; Dupont, T. F.; Huber, G., Capillary flow as the cause of ring stains from dried liquid drops. *Nature* **1997,** *389* (6653), 827.
16. Deegan, R. D., Pattern formation in drying drops. *Physical review E* **2000,** *61* (1), 475.
17. Deegan, R. D.; Bakajin, O.; Dupont, T. F.; Huber, G.; Nagel, S. R.; Witten, T. A., Contact line deposits in an evaporating drop. *Physical review E* **2000,** *62* (1), 756.
18. Hu, H.; Larson, R. G., Marangoni effect reverses coffee-ring depositions. *The Journal of Physical Chemistry B* **2006,** *110* (14), 7090-7094.
19. Hu, H.; Larson, R. G., Analysis of the effects of Marangoni stresses on the microflow in an evaporating sessile droplet. *Langmuir* **2005,** *21* (9), 3972-3980.
20. Ristenpart, W. D.; Kim, P. G.; Domingues, C.; Wan, J.; Stone, H. A., Influence of substrate conductivity on circulation reversal in evaporating drops. *Physical Review Letters* **2007,** *99* (23), 234502.

21. Xu, X.; Luo, J.; Guo, D., Criterion for Reversal of Thermal Marangoni Flow in Drying Drops. *Langmuir the Acs Journal of Surfaces & Colloids* **2010,** *26* (3), 1918-22.

22. Li, Y.; Yang, Q.; Li, M.; Song, Y., Rate-dependent interface capture beyond the coffee-ring effect. *Scientific reports* **2016,** *6*.

23. Nguyen, T. A. H.; Biggs, S. R.; Nguyen, A. V., Manipulating colloidal residue deposit from drying droplets: Air/liquid interface capture competes with coffee-ring effect. *Chemical Engineering Science* **2017,** *167*, 78-87.

24. Devlin, N. R.; Loehr, K.; Harris, M. T., The importance of gravity in droplet evaporation: A comparison of pendant and sessile drop evaporation with particles. *AIChE Journal* **2016,** *62* (3), 947-955.

25. Sandu, I.; Fleaca, C. T., The influence of gravity on the distribution of the deposit formed onto a substrate by sessile, hanging, and sandwiched hanging drop evaporation. *Journal of colloid and interface science* **2011,** *358* (2), 621-625.

26. Li, Y.-F.; Sheng, Y.-J.; Tsao, H.-K., Evaporation stains: suppressing the coffee-ring effect by contact angle hysteresis. *Langmuir* **2013,** *29* (25), 7802-7811.

27. Dunn, A.; Wasley, T. J.; Li, J.; Kay, R. W.; Stringer, J.; Smith, P. J.; Esenturk, E.; Connaughton, C.; Shephard, J. D., Laser textured superhydrophobic surfaces and their applications for homogeneous spot deposition. *Applied Surface Science* **2016,** *365*, 153-159.

28. Patil, N. D.; Bange, P. G.; Bhardwaj, R.; Sharma, A., Effects of Substrate Heating and Wettability on Evaporation Dynamics and Deposition Patterns for a Sessile Water Droplet Containing Colloidal Particles. *Langmuir the Acs Journal of Surfaces & Colloids* **2016,** *32* (45).

29. Yu, Y. S.; Wang, M. C.; Huang, X., Evaporative deposition of polystyrene microparticles on PDMS surface. *Scientific Reports* **2017,** *7* (1).

30. Askounis, A.; Sefiane, K.; Koutsos, V.; Shanahan, M. E. R., The effect of evaporation kinetics on nanoparticle structuring within contact line deposits of volatile drops. *Colloids & Surfaces A Physicochemical & Engineering Aspects* **2014,** *441* (3), 855-866.

31. Bhardwaj, R.; Patil, N.; Sharma, A. In *Self-sorting of bi-dispersed colloidal particles near contact line of an evaporating sessile droplet*, APS Meeting, 2018.

32. Yunker, P. J.; Still, T.; Lohr, M. A.; Yodh, A., Suppression of the coffee-ring effect by shape-dependent capillary interactions. *Nature* **2011,** *476* (7360), 308-311.

33. Larson, R. G., Transport and deposition patterns in drying sessile droplets. *AIChE Journal* **2014,** *60* (5), 1538-1571.

34. Sefiane, K., Patterns from drying drops. *Advances in colloid and interface science* **2014,** *206*, 372-381.

35. Marin, A.; Liepelt, R.; Rossi, M.; Kähler, C. J., Surfactant-driven flow transitions in evaporating droplets. *Soft Matter* **2016,** *12* (5), 1593-1600.

36. Barmi, M. R.; Meinhart, C. D., Convective flows in evaporating sessile droplets. *Journal of Physical Chemistry B* **2014,** *118* (9), 2414-21.

37. Parsa, M.; Harmand, S.; Sefiane, K.; Bigerelle, M.; Deltombe, R., Effect of Substrate Temperature on Pattern Formation of Nanoparticles from Volatile Drops. *Langmuir* **2015,** *31* (11), 3354-67.

38. Weon, B. M.; Je, J. H., Fingering inside the coffee ring. *Physical Review E* **2013,** *87* (1), 013003.

39. Shen, X.; Ho, C.-M.; Wong, T.-S., Minimal size of coffee ring structure. *The Journal of Physical Chemistry B* **2010,** *114* (16), 5269-5274.

40. Bhardwaj, R.; Fang, X.; Somasundaran, P.; Attinger, D., Self-assembly of colloidal particles from evaporating droplets: role of DLVO interactions and proposition of a phase diagram. *Langmuir* **2010,** *26* (11), 7833-7842.

41. Li, W.; Lan, D.; Sun, H.; Wang, Y., Drop capturing based on patterned substrate in space. *Langmuir* **2018,** *34* (16), 4715-4721.

42. Gennes, P. G. D.; Brochard-Wyart, F.; Quéré, D., *Capillarity and Gravity*. Springer New York: 2004; p 33-67.

43. Li, W.; Lan, D.; Wang, Y., Dewetting-mediated pattern formation inside the coffee ring. *Physical Review E* **2017,** *95* (4), 042607.

44. Bigioni, T. P.; Lin, X.-M.; Nguyen, T. T.; Corwin, E. I.; Witten, T. A.; Jaeger, H. M., Kinetically driven self assembly of highly ordered nanoparticle monolayers. *Nature materials* **2006,** *5* (4), 265.

45. Rhodes, M. J., *Introduction to particle technology*. John Wiley & Sons: 2008.

46. Sobac, B.; Brutin, D., Thermal effects of the substrate on water droplet evaporation. *Physical Review E* **2012,** *86* (2), 021602.

47. Marín, Á. G.; Gelderblom, H.; Lohse, D.; Snoeijer, J. H., Order-to-disorder transition in ring-shaped colloidal stains. *Physical review letters* **2011,** *107* (8), 085502.

TOC Graphic

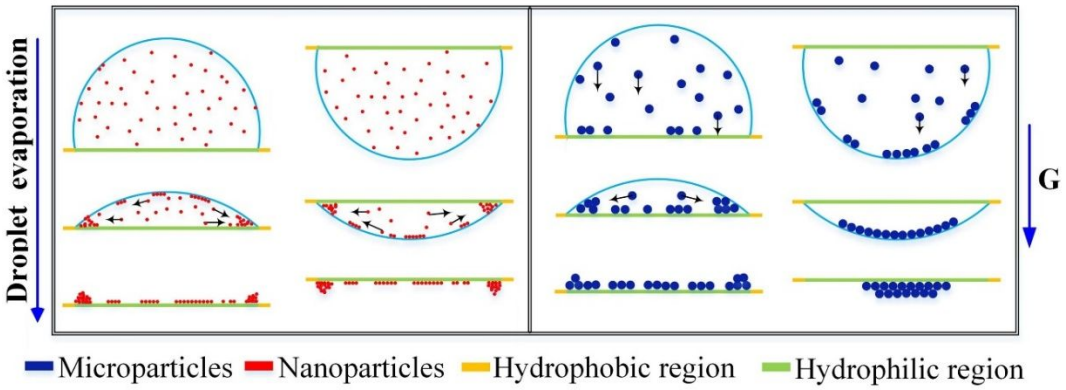

Patterns formation in evaporation of the sessile and pendant droplets: interactions of gravitational sedimentation, interface shrinkage and capillary flow.

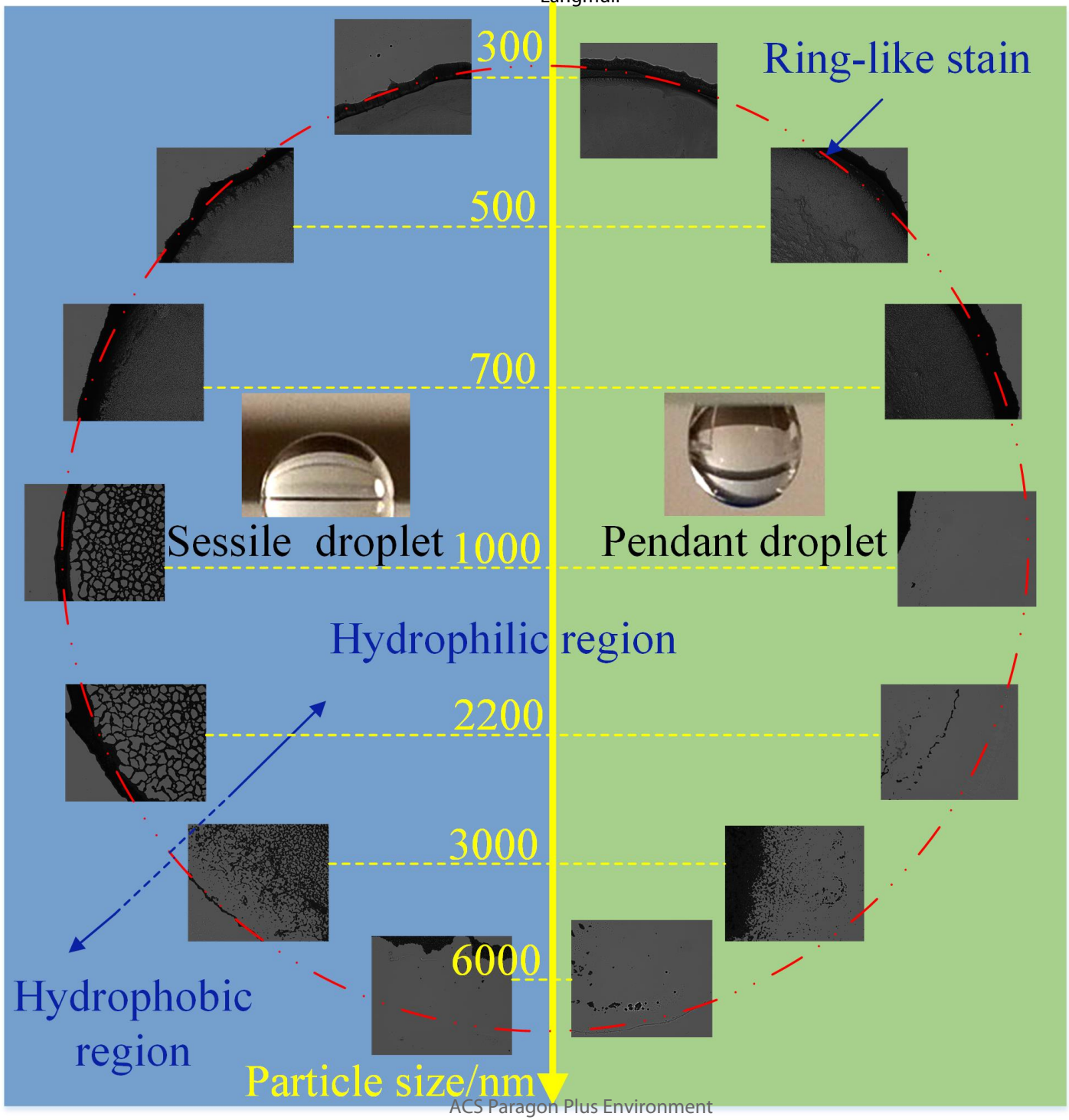
300
Ring-like stain
500
700
Sessile droplet
Pendant droplet
1000
Hydrophilic region
2200
3000
6000
Hydrophobic region
Particle size/nm

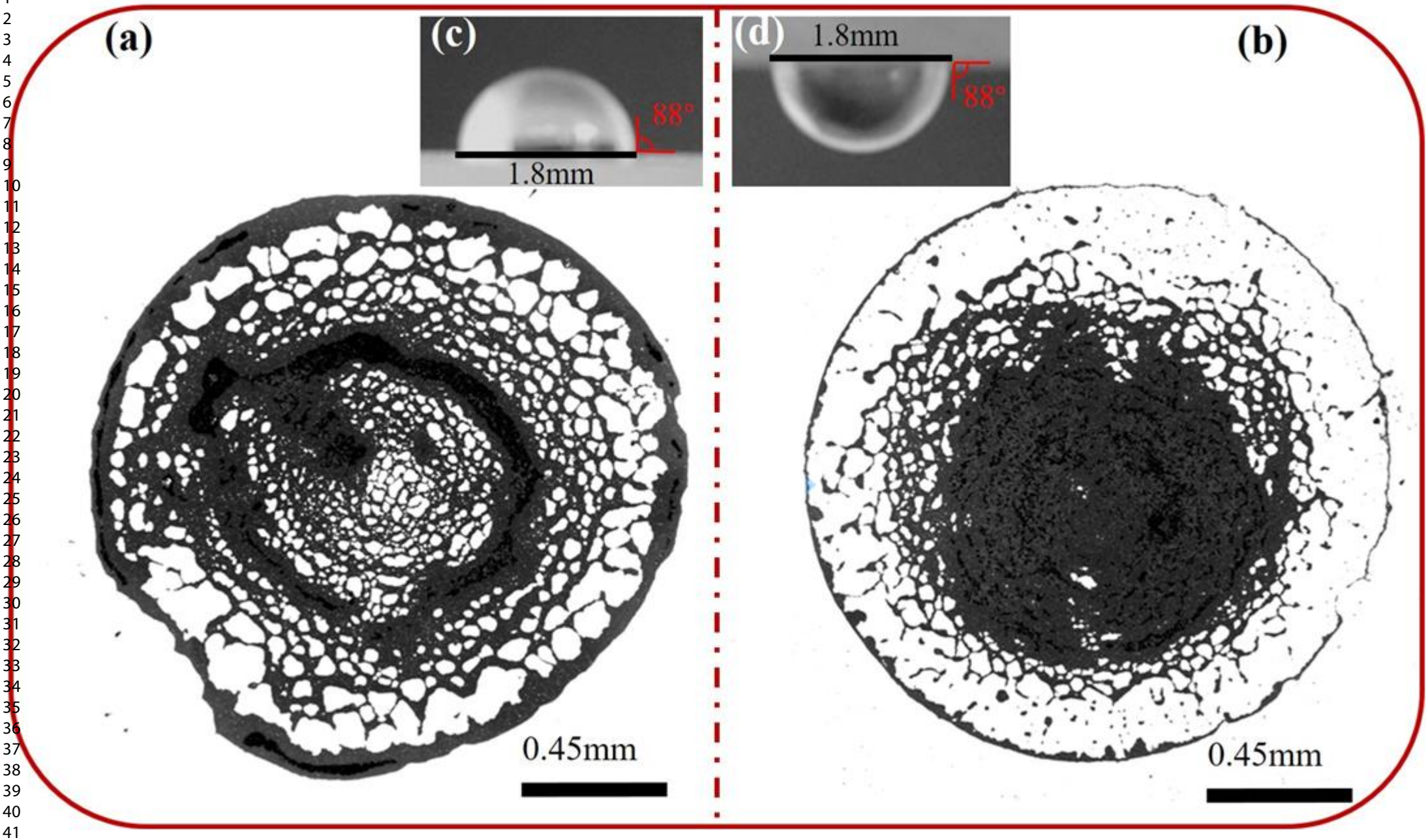
(a)
(c)
88°
1.8mm
(d)
1.8mm
88°
(b)
0.45mm
0.45mm

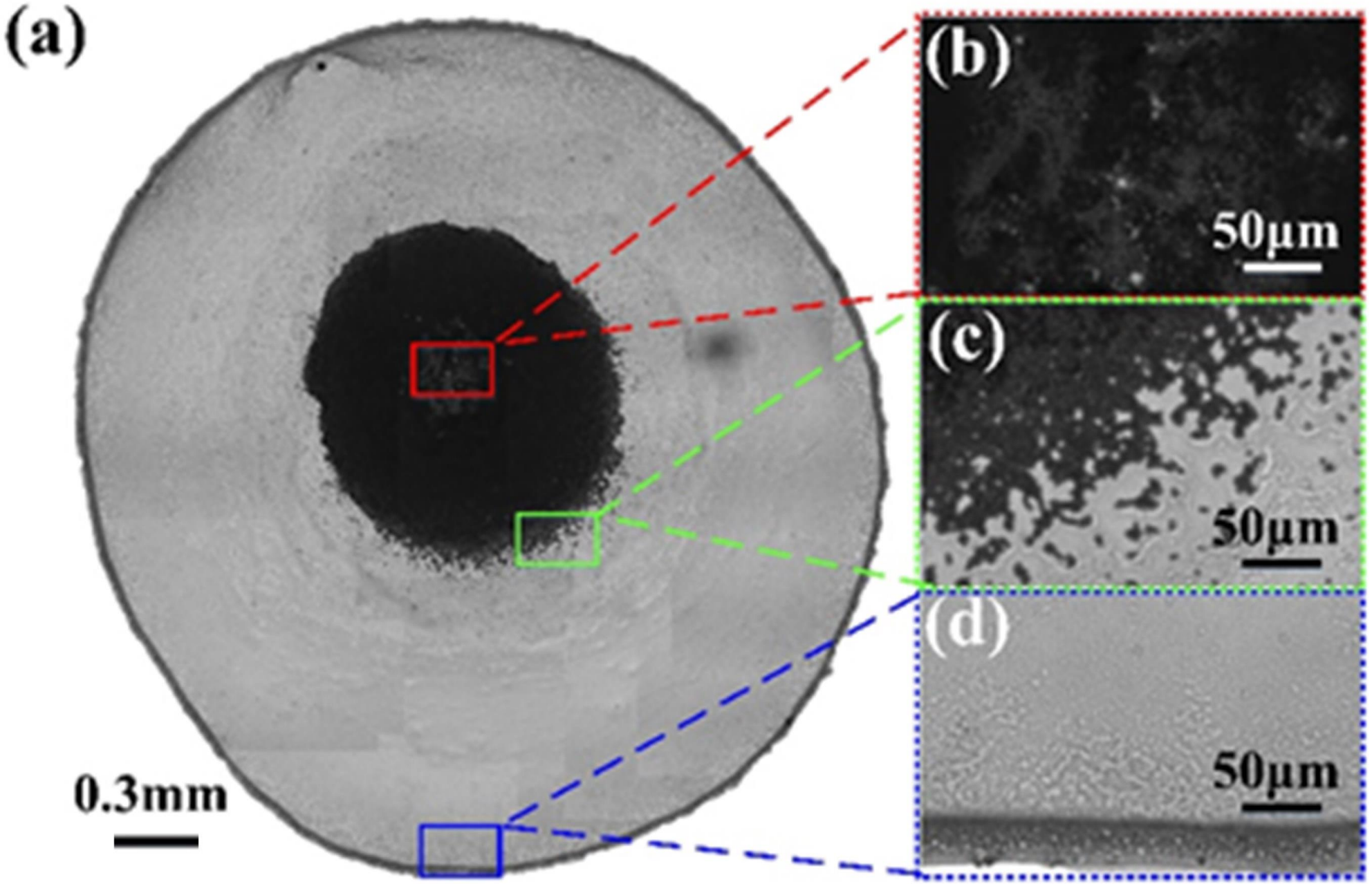
(a)
0.3mm
(b)
50μm
(c)
50μm
(d)
50μm

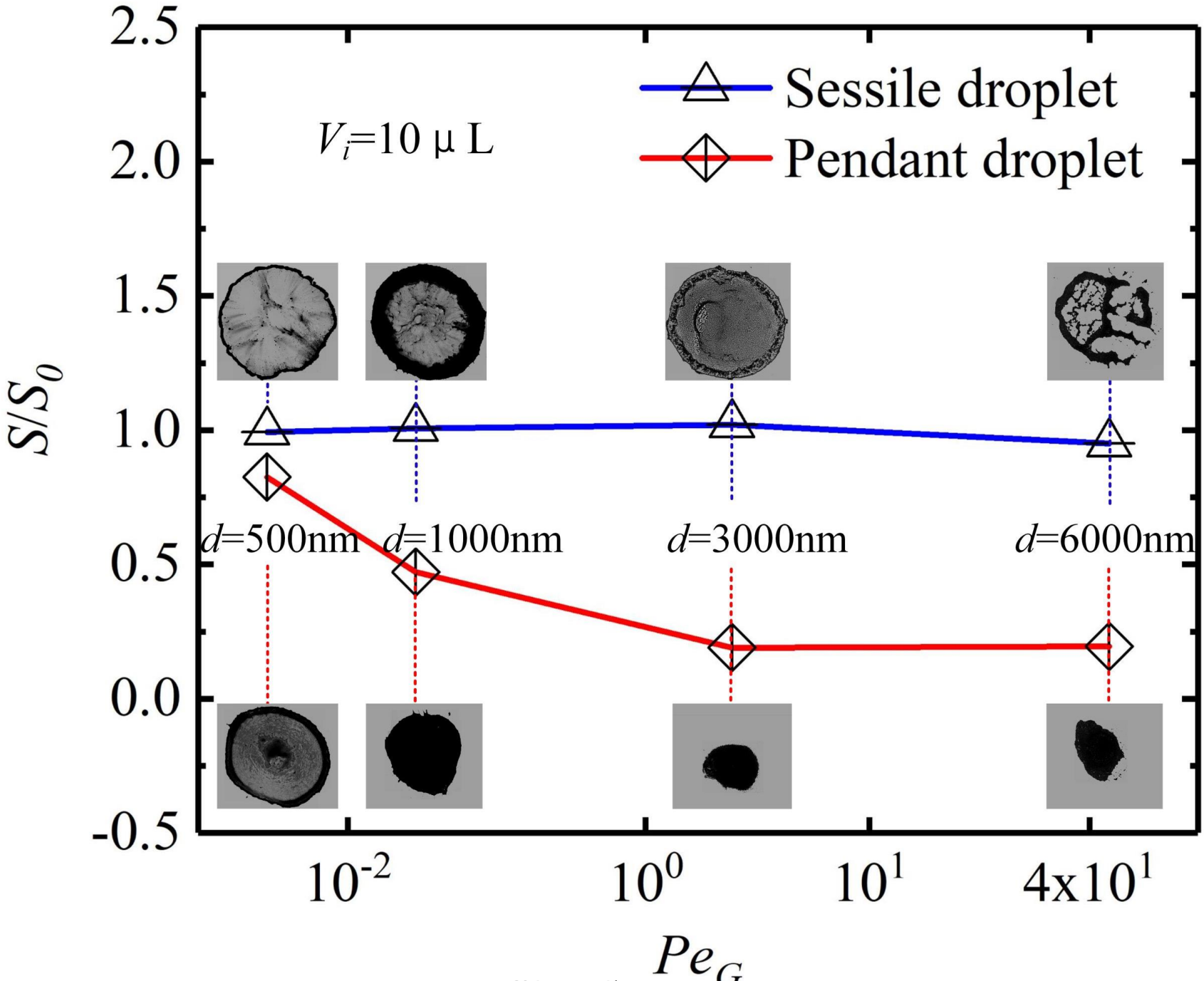
2.5
2.0
1.5
1.0
0.5
0.0
-0.5
S/S0
Vi=10 μ L
Sessile droplet
Pendant droplet
d=500nm
d=1000nm
d=3000nm
d=6000nm
10-2
100
101
4x101
PeG

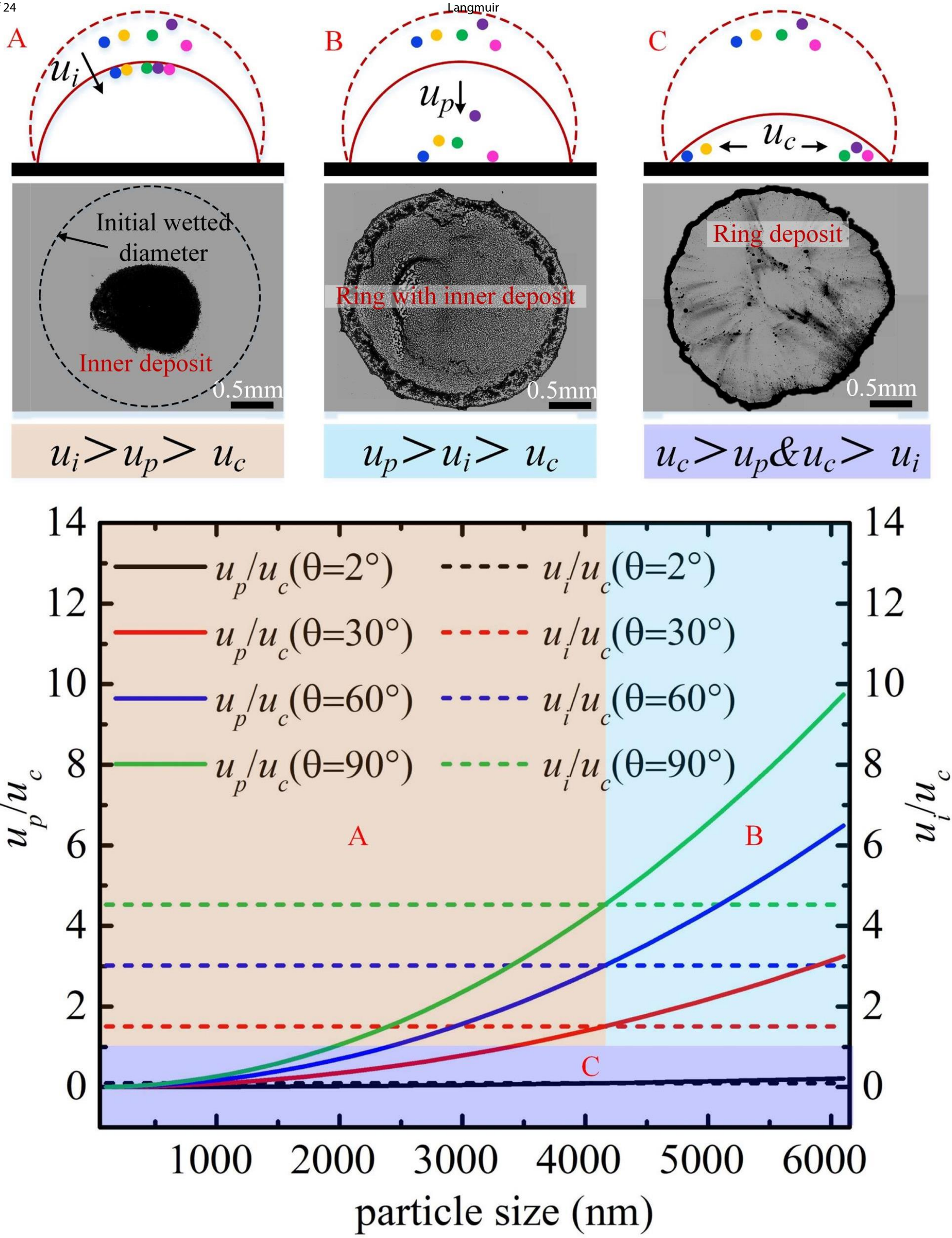
A
B
C
u_i
u_p
u_c
Initial wetted diameter
Inner deposit
Ring with inner deposit
Ring deposit
0.5mm
0.5mm
0.5mm
$u_i > u_p > u_c$
$u_p > u_i > u_c$
$u_c > u_p \& u_c > u_i$
$u_p/u_c(\theta=2°)$
$u_p/u_c(\theta=30°)$
$u_p/u_c(\theta=60°)$
$u_p/u_c(\theta=90°)$
$u_i/u_c(\theta=2°)$
$u_i/u_c(\theta=30°)$
$u_i/u_c(\theta=60°)$
$u_i/u_c(\theta=90°)$
u_p/u_c
u_i/u_c
0
2
4
6
8
10
12
14
1000
2000
3000
4000
5000
6000
particle size (nm)

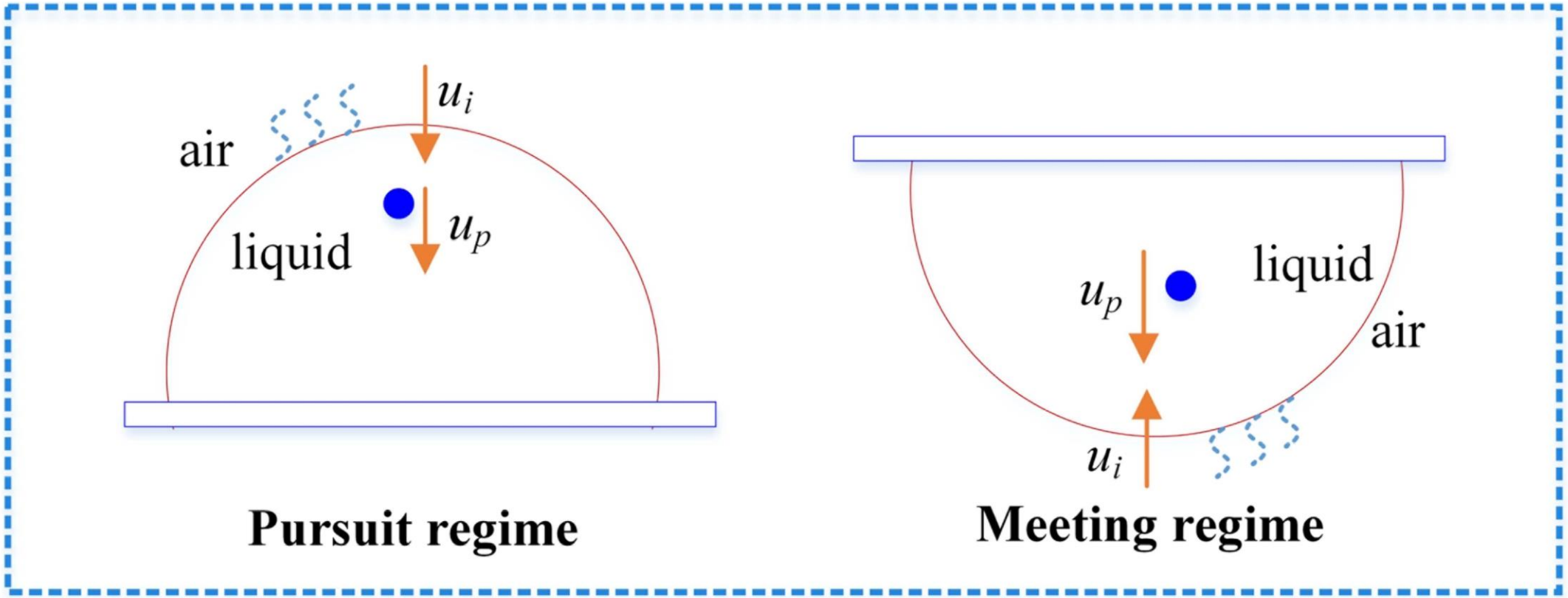
air
u_i
liquid
u_p
Pursuit regime
u_p
liquid
air
u_i
Meeting regime

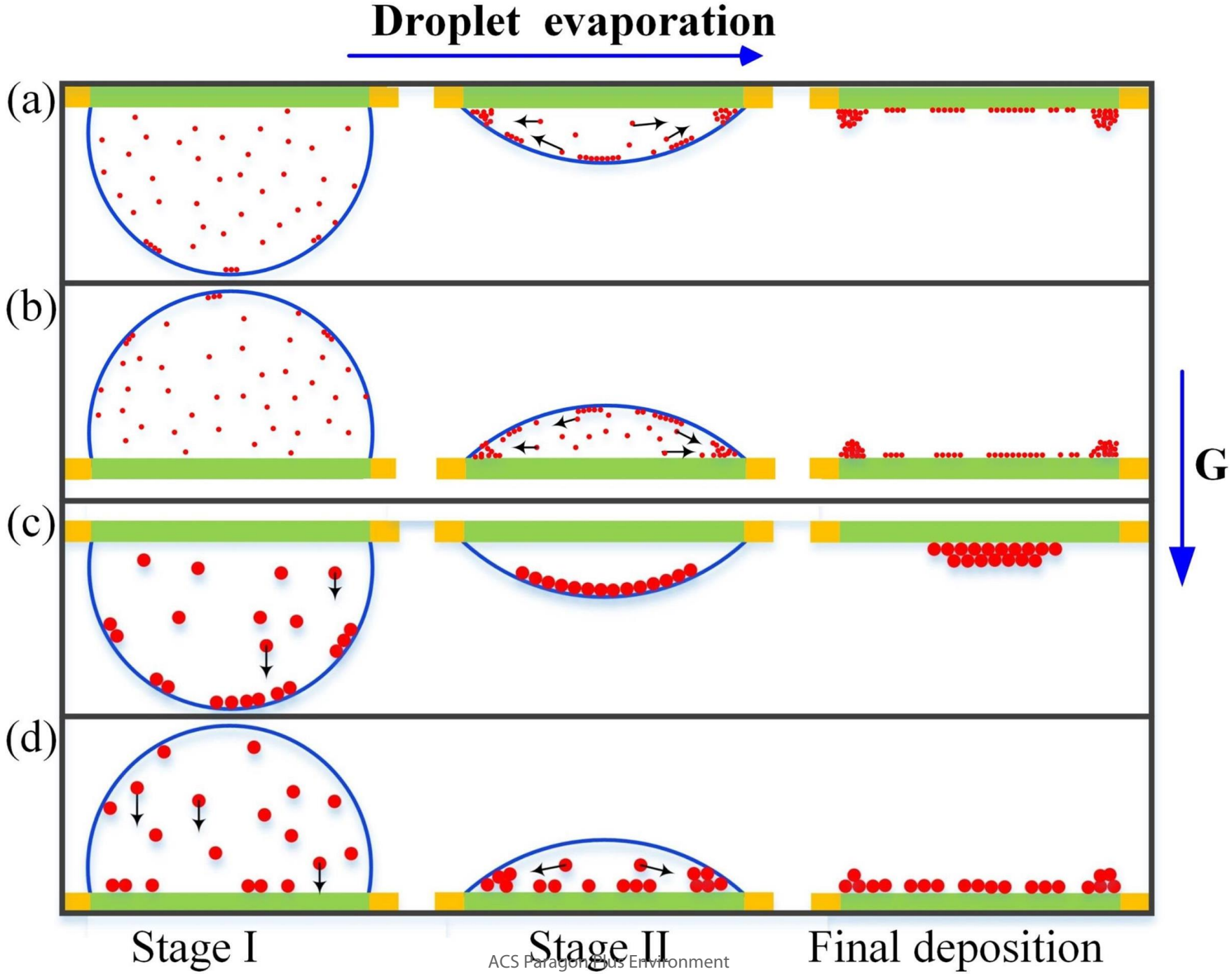

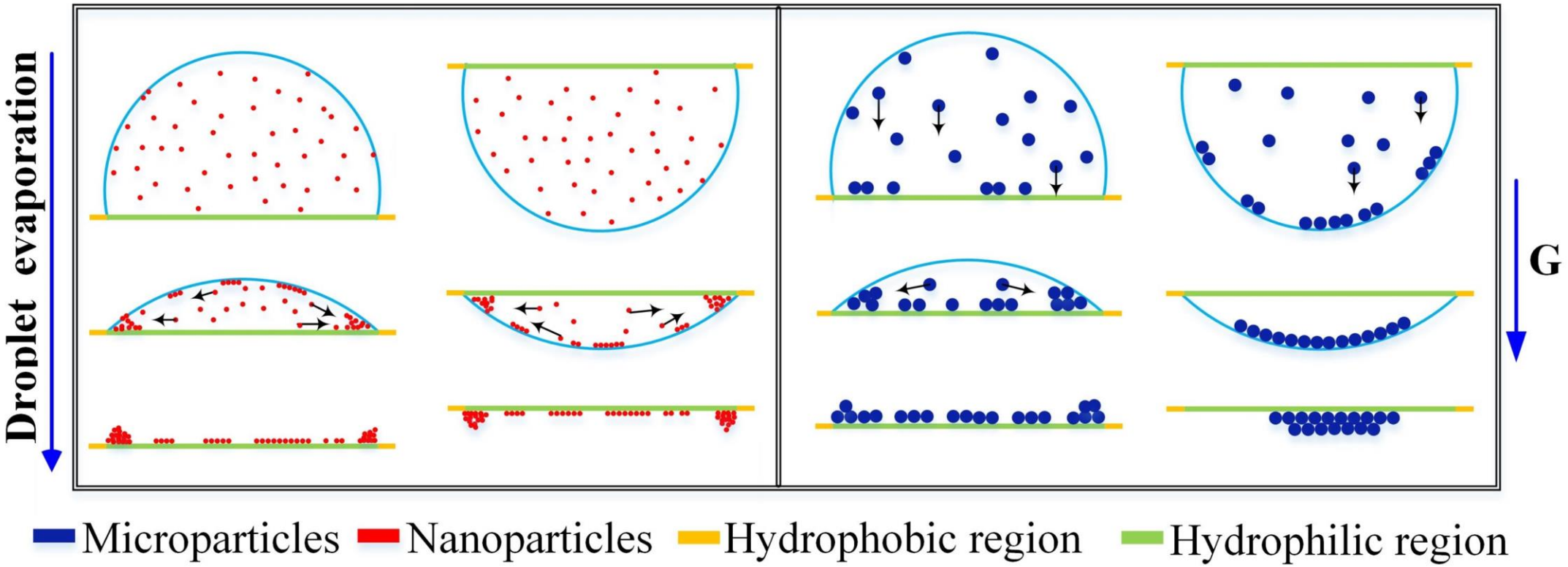
Droplet evaporation
G
Microparticles
Nanoparticles
Hydrophobic region
Hydrophilic region